

## ASSESSING SELF-ABSORBED MOLECULAR LINES AS TRACERS OF GRAVITATIONAL COLLAPSE

LILLIAN Y. CAI<sup>\* 1,2</sup>, FELIX D. PRIESTLEY<sup>1</sup>, AND SARAH E. RAGAN<sup>1</sup>School of Physics and Astronomy, Cardiff University, Queen's Buildings, The Parade, Cardiff CF24 3AA, UK and  
Department of Astrophysical Sciences, Princeton University, Princeton, NJ, USA(Dated: July 2025)  
Version October 1, 2025

## ABSTRACT

Redshifted self-absorption features in molecular lines are commonly interpreted as signatures of gravitational collapse in pre- and protostellar cores. The shape of the line profile then encodes information on the dynamics of the collapse. There exist well-established observational techniques to estimate infall velocities from these profiles, but these have historically been calibrated on constant-velocity slab models, whereas more realistic simulations of gravitational collapse produce highly non-uniform radial velocity profiles. We produce synthetic line observations of a simulated collapsing prestellar core, including a treatment of the time-dependent chemical evolution. Applying observational techniques to the synthetic line profiles, we find that the estimated infall velocities are significantly and systematically lower than the mass-weighted infall velocities from the simulation. This is primarily because the self-absorption features tend to originate from the outer regions of the core, well beyond the location of the peak infall velocity. Velocities and mass accretion rates measured via these techniques are likely to underestimate the true values.

*Subject headings:* astrochemistry – stars: formation – ISM: molecules

## 1. INTRODUCTION

Dynamical evolution in molecular clouds takes place over timescales of millions of years (Bergin & Tafalla 2007), making it impossible to directly observe the collapse of material to stellar densities. A key indirect observational signature of star formation activity is redshifted self-absorption in molecular line profiles (e.g. Lee et al. 1999, 2001; Tafalla et al. 1998), interpreted as arising from infalling foreground material along the line of sight. While there are some caveats to this interpretation (e.g. Smith et al. 2012), these features remain widely used to identify regions of molecular clouds undergoing gravitational collapse (Campbell et al. 2016; Redaelli et al. 2022).

Beyond simply identifying that collapse is occurring, self-absorbed line profiles provide quantitative information as to the nature of this collapse. Myers et al. (1996) demonstrated a simple analytical method to estimate infall velocities from line profile shapes. A few additional assumptions provide the mass infall rate, which can be used to discriminate between competing theories of star formation (Mac Low & Klessen 2004).

While the simplicity of this model makes it attractive, it also necessarily limits its accuracy when applied to more complex situations. De Vries & Myers (2005) previously investigated this topic, and presented some modifications to improve the original Myers et al. (1996) method's accuracy, allowing for a non-uniform excitation temperature. However, this was still within the context of a model with a single-valued infall velocity, whereas gravitational collapse will in general produce a radially-varying infall velocity even in the simplest cases (Larson 1969). Moreover, different molecular lines will tend to probe different parts of this velocity profile, further com-

plicating the situation (Smith et al. 2013; Chira et al. 2014; Keown et al. 2016).

In this paper, we combine hydrodynamical simulations with time-dependent chemistry and radiative transfer to produce synthetic line observations of model prestellar cores. We then obtain infall velocities from the line emission using established observational techniques, and assess how these values correspond to the underlying velocities in the simulation. We find that measured infall velocities tend to underestimate the true mass-weighted value, often by a significant margin, and so should be treated with some caution.

## 2. METHOD

We performed smoothed-particle hydrodynamic (SPH) simulations of a collapsing prestellar core using PHANTOM (Price et al. 2018). Our initial conditions are a critical Bonnor-Ebert sphere (Bonnor 1956; Ebert 1957) with mass  $5 M_{\odot}$ , radius 0.221 pc and sound speed  $0.2 \text{ km s}^{-1}$  (i.e. molecular gas at 10 K), embedded in a background medium with a density 20 times lower than the sphere's edge and sound speed raised to ensure pressure equilibrium. We use a particle mass of  $2.7 \times 10^{-5} M_{\odot}$ , giving  $\sim 2 \times 10^5$  particles within the sphere. We increase the sphere's mass by 10% to induce immediate collapse, and follow its evolution for 0.87 Myr, at which point the central density has reached  $10^7 \text{ cm}^{-3}$ .

We select all particles with a final radius within 0.2 pc of the core's centre, and use their evolutionary histories as input for UCLCHEM (Holdship et al. 2017), a time-dependent gas-grain chemical code, thereby obtaining self-consistent molecular abundance profiles rather than the constant values adopted in previous work.. We use the UMIST12 (McElroy et al. 2013) reaction network and elemental abundances listed in Table 1. The cosmic ray

\*email: lc5846@princeton.edu

TABLE 1  
ELEMENTAL ABUNDANCES USED IN THE CHEMICAL MODELLING.

Element	Abundance	Element	Abundance
C	$1.4 \times 10^{-4}$	S	$1.2 \times 10^{-5}$
N	$7.6 \times 10^{-5}$	Si	$1.5 \times 10^{-7}$
O	$3.2 \times 10^{-4}$	Mg	$1.4 \times 10^{-7}$

ionisation rate is taken to be  $1.3 \times 10^{-17} \text{ s}^{-1}$ , and we assume the core is sufficiently embedded within its parent cloud that the external ultraviolet (UV) radiation field is completely attenuated; internal UV photons produced by cosmic rays are included.

We then performed radiative transfer modelling of the core's line emission using RADMC3D (Dullemond et al. 2012). The SPH particle data are interpolated onto a 0.4 pc Cartesian grid using SPLASH (Price 2007), and each cell is assigned the molecular abundances of the nearest post-processed SPH particle to the cell centre. Collisional data are taken from the LAMDA database (Schöier et al. 2005). We model the  $J = 1 - 0$  rotational transitions of  $\text{C}^{18}\text{O}$ ,  $\text{N}_2\text{H}^+$ ,  $\text{HCO}^+$  and  $\text{H}^{13}\text{CO}^+$ , and the  $J = 2 - 1$  transitions of CS and  $\text{C}^{34}\text{S}$ ; as the reaction network does not include the rarer isotopes ( $^{13}\text{C}$ ,  $^{18}\text{O}$  and  $^{34}\text{S}$ ), we scale the abundances of the main isotopologue by the isotopic ratios in Wilson & Rood (1994), and assume identical collisional rates. Our output position-position-velocity cubes have spatial resolution  $2 \times 10^{-3}$  pc and velocity resolution  $3 \times 10^{-3} \text{ km s}^{-1}$ . We obtain line profiles by averaging the emission within circular apertures of radius 0.2 and 0.05 pc.

Using data from the line profiles, we calculate the infall velocity for each combination of species. CS and  $\text{HCO}^+$  are our optically thick self-absorbed lines,  $\text{N}_2\text{H}^+$  and  $\text{C}^{18}\text{O}$  are optically thin, and  $\text{C}^{34}\text{S}$  and  $\text{H}^{13}\text{CO}^+$  are to make sure our results aren't just due to chemical differences between optically thick and thin tracers. We find the infall velocities for apertures of radius 0.2 and 0.05 pc, and timesteps 0.81 Myr and 0.87 Myr. While the time interval is small in astronomical terms, this spans a period of rapid evolution in the model's density and velocity profiles. From Myers et al. (1996), we use the following equation:

$$V_{in} \approx \frac{\sigma_{bulk}^2}{v_{red} - v_{blue}} \ln \left( \frac{1 + eT_{BD}/T_D}{1 + eT_{RD}/T_D} \right), \quad (1)$$

where each of the parameters, listed in Table 2 and depicted in Fig. 1a, can be obtained from the line profiles. From CS and  $\text{HCO}^+$ , which have a prominent self-absorption dip compared to the other species, we can obtain most of the parameters using the blue and red peaks.  $v_{blue}$  and  $v_{red}$  are the velocities at the blue and red peaks from the dip,  $T_{BD}$  and  $T_{RD}$  are the heights of their respective peaks above the dip, and  $T_D$  is the brightness temperature of the dip.  $\text{N}_2\text{H}^+$  and  $\text{C}^{18}\text{O}$ , as well as  $\text{C}^{34}\text{S}$  and  $\text{H}^{13}\text{CO}^+$ , are more optically thin so they are used to obtain the non-thermal velocity dispersions. We fit a Gaussian distribution to their line profiles, masking the self-absorption dip if present, as illustrated in Fig. 1b.

Each fitted curve has a standard deviation, which is taken as the observed velocity dispersion. We use this to calculate  $\sigma_{bulk}$ , the bulk velocity dispersion, using the equation  $\sigma_{bulk}^2 = \sigma_{obs}^2 - \sigma_{therm}^2$ , where  $\sigma_{therm}^2 = kT/m$ ,

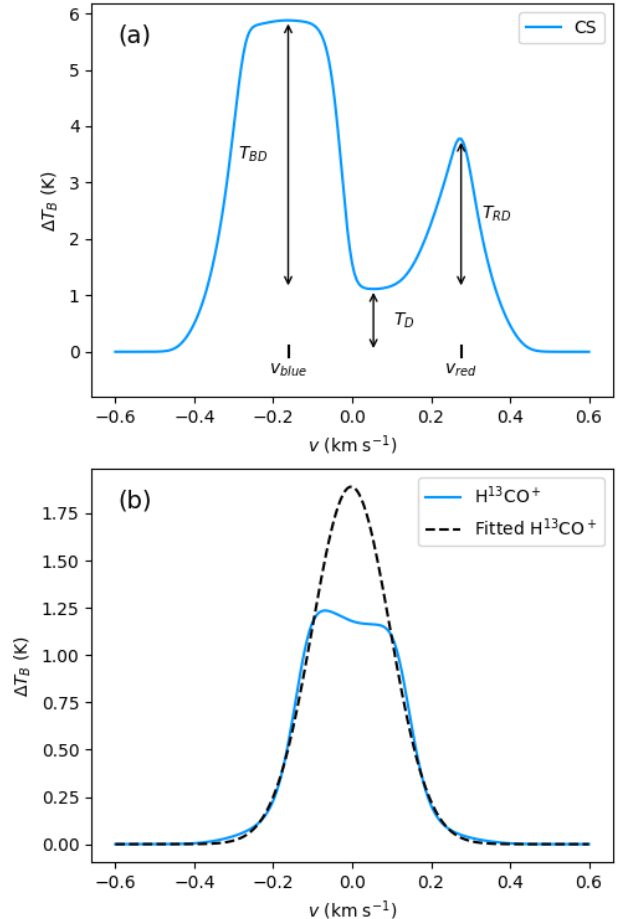


FIG. 1.— Top: Line profile parameters in Eq. 1. Bottom: Example of fitting a Gaussian function to a self-absorbed line profile.

where  $m$  is the molecular mass and  $k$  is the Boltzmann constant. We set  $T = 10\text{K}$ , to obtain the  $\sigma$  values that go into the infall velocity equation.

### 3. RESULTS

Fig. 2 displays the radial velocity and density profiles at both 0.81 Myr and 0.87 Myr. While the densities reach similar values at the sphere's edge, about  $3.0 - 3.3 \times 10^2 \text{ cm}^{-3}$ , the central density of the final timestep is over an order of magnitude larger than the central density at 0.81 Myr, which levels off at  $4.6 \times 10^5 \text{ cm}^{-3}$ . The radial velocity profiles both have a clear peak infall velocity, but the velocity profile at 0.87 Myr is noticeably broader and reaches a larger maximum by a factor of about 1.7 compared to the 0.81 Myr curve. Fig. 3 shows that all 4 of the abundance profiles remain similar across both timesteps. The abundances decrease by at most one order of magnitude toward the center of the sphere, beginning at  $r = 10^{-2}$  pc, due to freeze-out; however, this does not occur for  $\text{N}_2\text{H}^+$  (Tafalla et al. 2002, 2004).

TABLE 2  
PARAMETERS USED TO CALCULATE  $V_{in}$ .

r = 0.05 pc, t = 0.81 Myr					r = 0.2 pc, t = 0.81 Myr						
Species	$v_{red}$	$v_{blue}$	$T_D$	$T_{RD}$	$T_{BD}$	Species	$v_{red}$	$v_{blue}$	$T_D$	$T_{RD}$	$T_{BD}$
HCO+	0.2640	-0.1860	2.3652	1.6921	5.0150		0.1860	-0.1680	2.3394	0.1467	1.7453
CS	0.2460	-0.1740	1.1102	3.0850	4.8977		0.0840	-0.0960	1.0827	0.0060	1.8752
Species					Bulk Velocity ( $\sigma_{bulk}$ )						
N2H+			0.1073							0.0848	
H13CO+			0.1030							0.0728	
C18O			0.1015							0.0885	
C34S			0.1110							0.1001	
r = 0.05 pc, t = 0.87 Myr					r = 0.2 pc, t = 0.87 Myr						
Species	$v_{red}$	$v_{blue}$	$T_D$	$T_{RD}$	$T_{BD}$	Species	$v_{red}$	$v_{blue}$	$T_D$	$T_{RD}$	$T_{BD}$
HCO+	0.2940	-0.1920	2.3827	1.5441	4.8231		0.1860	-0.1740	2.2973	0.0736	1.4969
CS	0.2760	-0.1620	1.1134	2.6629	4.7633		0.0860	-0.0840	1.0757	-0.0216	1.4691
Species					Bulk Velocity ( $\sigma_{bulk}$ )						
N2H+			0.1486							0.0975	
H13CO+			0.1478							0.0807	
C18O			0.1267							0.1029	
C34S			0.1352							0.1078	

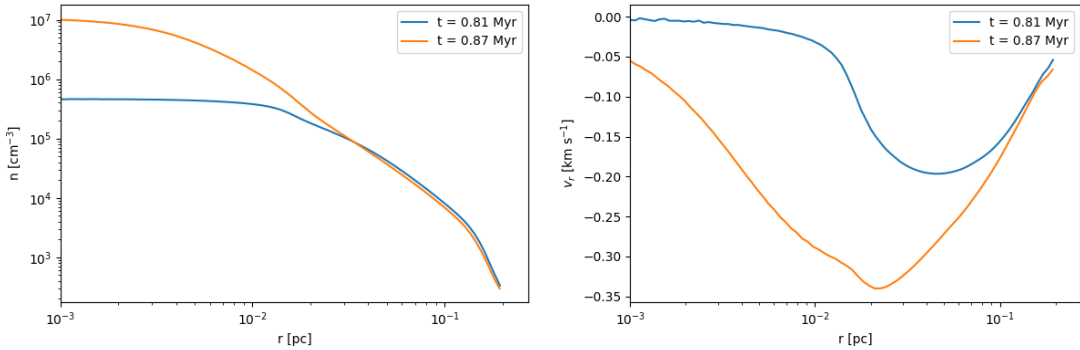


FIG. 2.— Density (left) and radial velocity (right) profiles at  $t = 0.81$  Myr and  $0.87$  Myr.

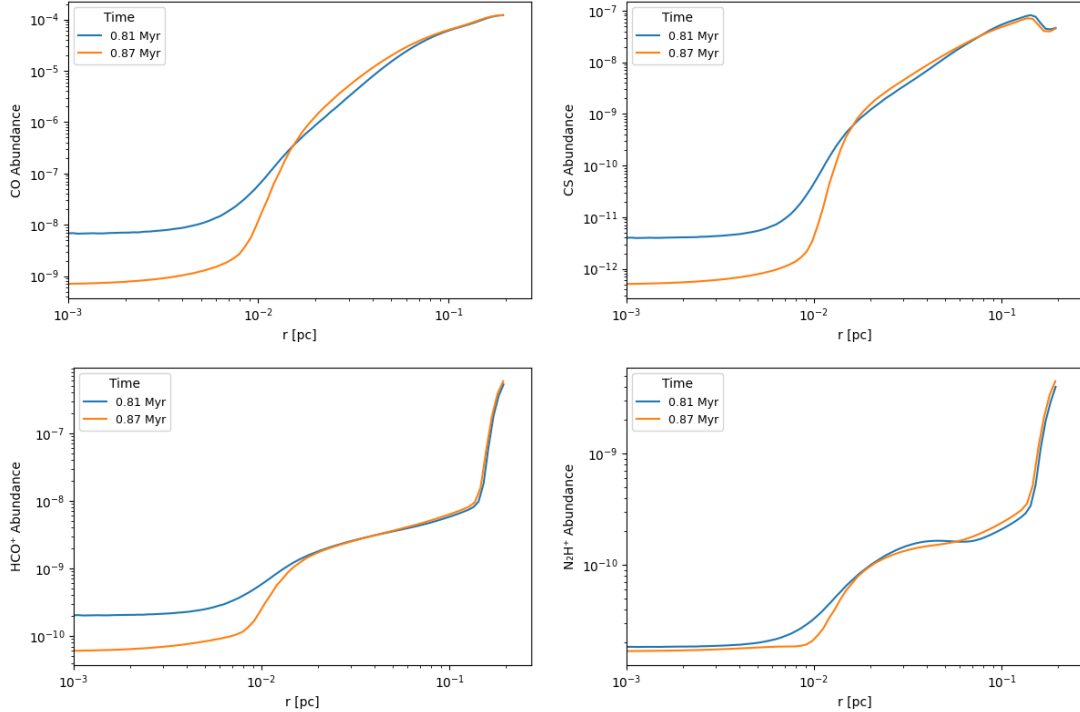


FIG. 3.— Abundances of CO (top left), CS (top right),  $\text{HCO}^+$  (bottom left), and  $\text{N}_2\text{H}^+$  (bottom right) versus hydrogen nuclei density at  $t = 0.81$  Myr and 0.87 Myr.

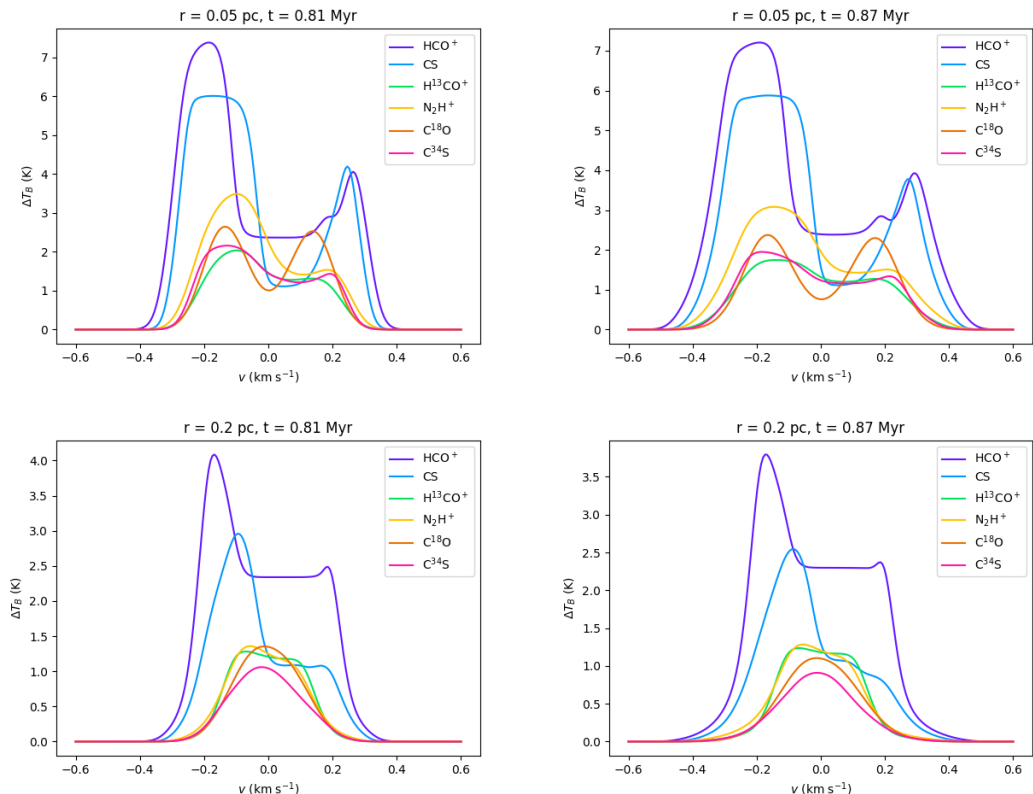


FIG. 4.— Line profiles for four combinations of radii and timesteps. Top Left:  $r = 0.05$  pc,  $t = 0.81$  Myr - Top Right:  $r = 0.05$  pc,  $t = 0.87$  Myr - Bottom Left:  $r = 0.2$  pc,  $t = 0.81$  Myr - Bottom Right:  $r = 0.2$  pc,  $t = 0.87$  Myr

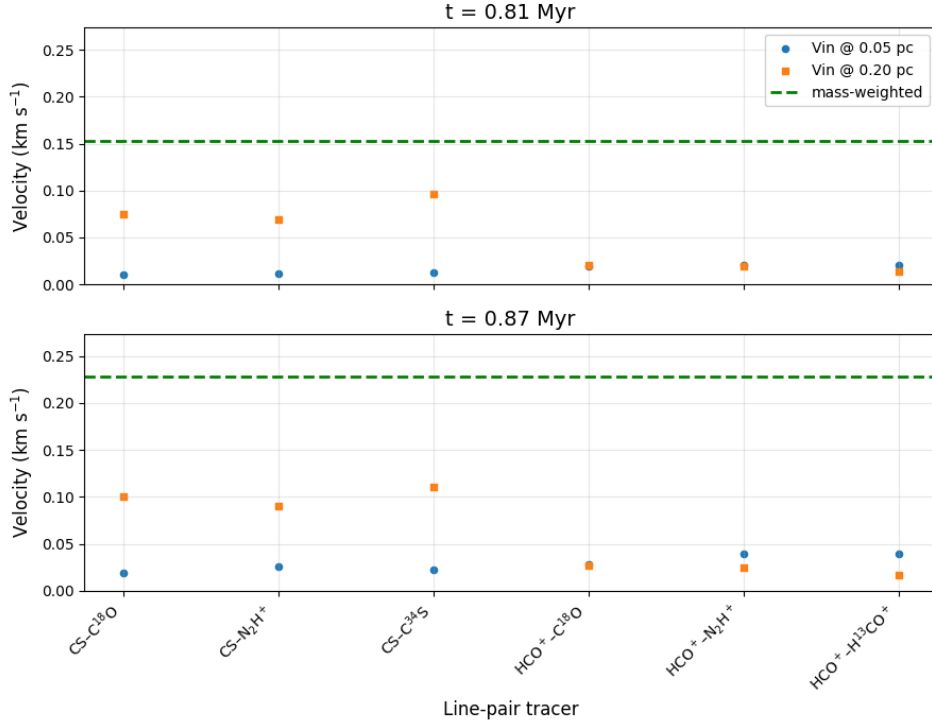


FIG. 5.— True mass-weighted velocity and calculated infall velocities for all line-pair tracers, at  $t = 0.81 \text{ Myr}$  and  $0.87 \text{ Myr}$ .

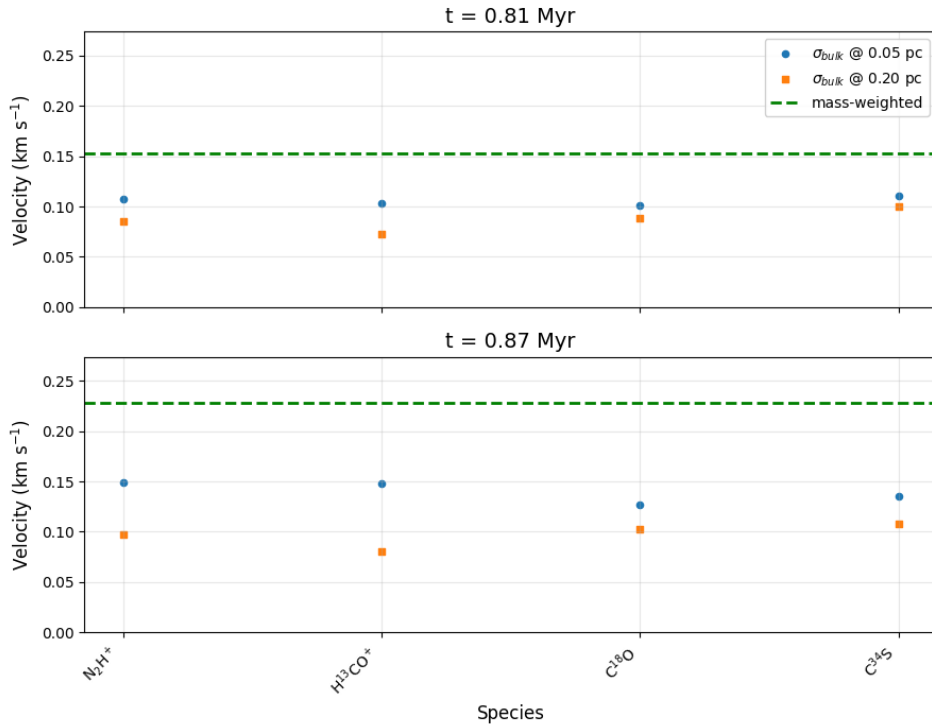


FIG. 6.— True mass-weighted velocity and bulk velocities for the optically thin species, at  $t = 0.81 \text{ Myr}$  and  $0.87 \text{ Myr}$ .

The line profiles for each of the radii and timestep combinations are shown in Fig. 4. Despite the physical differences between timesteps, the line profiles are fairly similar between 0.81 Myr and 0.87 Myr, but appear to vastly differ for different aperture sizes. At  $r = 0.05$  pc, each of the species  $\text{C}^{34}\text{S}$ ,  $\text{H}^{13}\text{CO}^+$ ,  $\text{N}_2\text{H}^+$ , and  $\text{C}^{18}\text{O}$  have much larger self-absorption dips, and the heights of the red and blue peaks of CS and  $\text{HCO}^+$  are also nearly twice of those at  $r = 0.2$  pc. In addition, the observed velocity dispersion is slightly larger at  $r = 0.05$  pc, although only by approximately a factor of 2.

Each of the infall velocities for the line-pair tracers, as well as the true mass-weighted velocities, are shown in Fig. 5. The infall velocities all fall significantly below the mass-weighted values of  $0.153 \text{ km s}^{-1}$  ( $t = 0.81$  Myr) and  $0.228 \text{ km s}^{-1}$  ( $t = 0.87$  Myr). Due to the similar line profile shapes, the Myers et al. (1996) method gives similar values of  $V_{in}$  for both timesteps, despite the later one having a significantly larger mass-weighted value. Using CS achieves results closest to the mass-weighted velocity, although only reaching about half the true value. On the other hand, using  $\text{HCO}^+$  often produces an infall velocity an entire order of magnitude smaller than the mass-weighted velocity. This discrepancy in results from using  $\text{HCO}^+$  is due to the velocities at the red and blue peaks being much farther apart compared to those of CS. This increases  $v_{red} - v_{blue}$  and produces a smaller  $V_{in}$ . The difference in results to those obtained from the CS line is despite the fact that the underlying velocity profile is identical, and arises purely from chemical and radiative transfer effects.

#### 4. DISCUSSION

Our results in Fig. 5 suggest that the Myers et al. (1996) method may underestimate infall velocities in prestellar cores by up to an order of magnitude, depending on the choice of lines and the area over which they are measured. As mass accretion rates estimated via this technique are linearly proportional to the measured  $V_{in}$ , they are subject to the same potentially-large source of error. While more sophisticated techniques have been developed (e.g. De Vries & Myers 2005), these are still calibrated using constant-velocity slab models, which we argue is the root cause of the discrepancy. For a two-slab model with a constant velocity, the velocity range of the self-absorption feature will naturally reflect this constant value. For more realistic structures, such as those

in Fig. 2, there is no guarantee that the self-absorption feature (essentially corresponding to an optical depth of unity) will originate at a velocity corresponding to the mass-weighted infall velocity, or any other appropriate measure of the ‘average’ infall rate. Lines from relatively-abundant molecules such as CS and  $\text{HCO}^+$  will likely have self-absorption features primarily originating in the outer regions of the core, where velocities are relatively low, thus underestimating the actual rate of infall.

We note that the non-thermal velocity dispersion measured from optically-thin lines is, in these simulations, entirely caused by infall motions, and typically within a factor of two of the actual mass-weighted infall velocity (Fig. 6). We suggest that in systems with red-shifted self-absorption features in optically-thick lines, the intrinsic velocity dispersion may be a better measure of the infall speed than values derived from line profile shapes, being largely unaffected by the issues discussed above. However, this interpretation may not hold in more complex, turbulent environments than the isolated collapsing cores considered here (Offner et al. 2008; Smith et al. 2012; Priestley et al. 2023, 2024), and future work should explore whether *any* observational signature is capable of probing the true mass-accretion rates of cores.

#### 5. CONCLUSION

We have used synthetic observations of a simulated prestellar core to investigate the connections between observational infall diagnostics and the actual rate of collapse of the core. We find that commonly-used techniques based on constant-velocity, two-slab models of line emission invariably underestimate the true infall velocity of the simulation. This is because realistic, non-uniform velocity profiles peak in the inner regions of the core and tend to zero at the edge; self-absorption features generally originate from radii beyond that of the peak velocity, and so produce systematically lower infall rates than the true mass-weighted value. Prestellar mass accretion rates derived via these techniques are therefore likely underestimating the true values by potentially an order of magnitude.

#### ACKNOWLEDGEMENTS

FDP and SER acknowledge the support of a consolidated grant (ST/W000830/1) from the UK Science and Technology Facilities Council (STFC).

#### REFERENCES

Bergin E. A., Tafalla M., 2007, *ARA&A*, **45**, 339  
 Bonnor W. B., 1956, *MNRAS*, **116**, 351  
 Campbell J. L., Friesen R. K., Martin P. G., Caselli P., Kauffmann J., Pineda J. E., 2016, *ApJ*, **819**, 143  
 Chira R.-A., Smith R. J., Klessen R. S., Stutz A. M., Shetty R., 2014, *Monthly Notices of the Royal Astronomical Society*, **444**, 874  
 De Vries C. H., Myers P. C., 2005, *ApJ*, **620**, 800  
 Dullemond C. P., Juhasz A., Pohl A., Sereshki F., Shetty R., Peters T., Commercon B., Flock M., 2012, RADMC-3D: A multi-purpose radiative transfer tool, *Astrophysics Source Code Library*, record ascl:1202.015 (ascl:1202.015)  
 Ebert R., 1957, *ZAp*, **42**, 263  
 Holdship J., Viti S., Jiménez-Serra I., Makrymallis A., Priestley F., 2017, *AJ*, **154**, 38  
 Keown J., et al., 2016, *ApJ*, **833**, 97  
 Larson R. B., 1969, *MNRAS*, **145**, 271  
 Lee C. W., Myers P. C., Tafalla M., 1999, *ApJ*, **526**, 788  
 Lee C. W., Myers P. C., Tafalla M., 2001, *ApJS*, **136**, 703  
 Mac Low M.-M., Klessen R. S., 2004, *Reviews of Modern Physics*, **76**, 125  
 McElroy D., Walsh C., Markwick A. J., Cordner M. A., Smith K., Millar T. J., 2013, *A&A*, **550**, A36  
 Myers P. C., Mardones D., Tafalla M., Williams J. P., Wilner D. J., 1996, *ApJ*, **465**, L133  
 Offner S. S. R., Krumholz M. R., Klein R. I., McKee C. F., 2008, *AJ*, **136**, 404  
 Price D. J., 2007, *PASA*, **24**, 159  
 Price D. J., et al., 2018, *PASA*, **35**, e031  
 Priestley F. D., Arzoumanian D., Whitworth A. P., 2023, *MNRAS*, **522**, 3890  
 Priestley F. D., Clark P. C., Glover S. C. O., Ragan S. E., Fehér O., Prole L. R., Klessen R. S., 2024, *MNRAS*, **531**, 4408

Redaelli E., Chacón-Tanarro A., Caselli P., Tafalla M., Pineda J. E., Spezzano S., Sipilä O., 2022, [ApJ](#), **941**, 168

Schöier F. L., van der Tak F. F. S., van Dishoeck E. F., Black J. H., 2005, [A&A](#), **432**, 369

Smith R. J., Shetty R., Stutz A. M., Klessen R. S., 2012, [ApJ](#), **750**, 64

Smith R. J., Shetty R., Beuther H., Klessen R. S., Bonnell I. A., 2013, [ApJ](#), **771**, 24

Tafalla M., Mardones D., Myers P. C., Caselli P., Bachiller R., Benson P. J., 1998, [ApJ](#), **504**, 900

This paper was built using the Open Journal of Astrophysics L<sup>A</sup>T<sub>E</sub>X template. The OJA is a journal which

Tafalla M., Myers P. C., Caselli P., Walmsley C. M., Comito C., 2002, [ApJ](#), **569**, 815

Tafalla M., Myers P. C., Caselli P., Walmsley C. M., 2004, [A&A](#), **416**, 191

Wilson T. L., Rood R., 1994, [ARA&A](#), **32**, 191

provides fast and easy peer review for new papers in the **astro-ph** section of the arXiv, making the reviewing process simpler for authors and referees alike. Learn more at <http://astro.theoj.org>.